

Strongly correlated proton-doped perovskite nickelate memory devices

Koushik Ramadoss¹, Fan Zuo¹, Yifei Sun¹, Zhen Zhang¹, Jianqiang Lin^{2,3}, Umesh Bhaskar⁴, SangHoon Shin⁴, Muhammad Ashraful Alam⁴, Supratik Guha^{2,3}, Dana Weinstein⁴ and Shriram Ramanathan¹

Abstract—We demonstrate memory devices based on proton doping and re-distribution in perovskite nickelates (RNiO_3 , $\text{R} = \text{Sm}, \text{Nd}$) that undergo filling-controlled Mott transition. Switching speeds as high as 30 ns in two-terminal devices patterned by electron-beam lithography is observed. The state switching speed reported here are $\sim 300\times$ greater than what has been noted with proton-driven resistance switching to date. The ionic-electronic correlated oxide memory devices also exhibit multi-state non-volatile switching. The results are of relevance to use of quantum materials in emerging memory and neuromorphic computing.

Index Terms—Nonvolatile memory, Resistive RAM, Thin film devices, Correlated oxides, Mott memory

I. INTRODUCTION

Resistive switching in oxides has the potential to enable high speed, densely scaled non-volatile memories for storage applications and emerging neuromorphic computing circuits [1]. These devices that form a part of RRAM technology are also being considered to replace NAND flash in the near future. RRAM usually involves a MIM structure whose resistance can be switched between low resistance state (LRS) and high resistance state (HRS) by application of a bias voltage. Many of these devices function based on the principle of local conductive filament formation or interface switching involving movement of oxygen vacancies in defective wide gap insulating oxides [1], [2]. At the same time, there is a need to innovate in new materials and physical phenomena for state switching, control of volatility and electric-field driven operation of memory devices without temperature constraints. In this work, we use proton-doped SmNiO_3 (SNO) and NdNiO_3 (NNO) as model strongly correlated quantum material systems to demonstrate high speed, non-volatile memory that do not require any forming voltage for its operation. Perovskite nickelates display collective properties like thermally-driven metal-insulator transition and anti-ferromagnetism and are being explored for various technologies such as sensing, photovoltaics and resistance switching [3], [4]. These materials

are weakly insulating (gap of the order of ~ 100 meV in the ground state). A large resistance change occurs due to proton-electron coupled doping from filling-control of Ni e_g orbitals in the nickelate leading to Mott transition that is distinct from any thermal phase transition [5]. This doping process is based on splitting of hydrogen into a proton and electron at a catalytic electrode like Pd, Pt resulting in the modification of Ni orbital occupancy that leads to an opening of large band gap (3 eV) when the Ni site occupancy changes from e_g^1 to e_g^2 . The protons reside in interstitial sites in the perovskite lattice. By applying voltage pulses, it is possible to realize distinct resistance states by spatially varying the dopant concentration with application of bias and the process is reversible. Orbital occupancy control via external electric field serves as the operational mechanism for these devices. While a mainstay topic of interest in physics, much work remains in exploring the potential of Mott transition in electronic devices. In this work we present the first demonstration of high speed non-volatile memory devices using nickelates, notably $300\times$ improvement in switching speed of protonic switches over what is reported in literature.

II. DEVICE FABRICATION

Thin films of SNO (50 nm) were grown on LaAlO_3 (LAO) substrates by RF co-sputtering from Sm and Ni targets and subsequently annealed under high pressure oxygen (1500 PSI) at 500°C to form the crystalline phase. The X-Ray diffraction of a pristine SNO film is shown in Fig. 1a. These un-doped films show a thermal insulator-metal transition around 402 K as shown in Fig. 1b. The thin films have a perovskite structure with optimal nickel valency of Ni^{3+} and can be catalytically doped with protons using metal electrodes (like Pt, Pd) on top of SNO and annealing in forming gas (Fig. 1c). During this process, the hydrogen breaks into proton and electron at the metal/SNO interface with the electron anchoring in the nickel orbitals changing the valence state from Ni^{3+} to Ni^{2+} , thus producing a strongly correlated electronic state. The process flow for fabricating these devices is shown in Fig. 1d. The fabrication of these memory cells starts with patterning pristine SNO films into rectangular bars using photolithography and then devices with either asymmetric electrodes (Ti/Au (10/100 nm) and Pd (100 nm)) or symmetric electrodes (Pd (100 nm)) were patterned to define a channel of width $100\text{ }\mu\text{m}$ and length $5\text{ }\mu\text{m}$. To fabricate sub-micron devices with channel length of few 100 nm, electron beam lithography was used for patterning. Protons are then doped

The authors acknowledge financial support from ARO W911NF-16-1-0289 and AFOSR FA9550-16-1-0159. This work was done in part at the Birk Nanotechnology Center, Purdue University.

K Ramadoss, F Zuo, Y Sun, Z Zhang and S Ramanathan are with the School of Materials Engineering, Purdue University, West Lafayette, IN 47907 USA (e-mail: koushikr.in@gmail.com).

U Bhaskar, D Weinstein, S Shin and M Alam are with the School of Electrical and Computer Engineering, Purdue University, West Lafayette, IN 47907 USA.

J Lin and S Guha are with the Center for Nanoscale Materials, Argonne National Laboratory, Lemont, IL 60439 USA and Institute for Molecular Engineering, University of Chicago, Chicago, IL 60615 USA

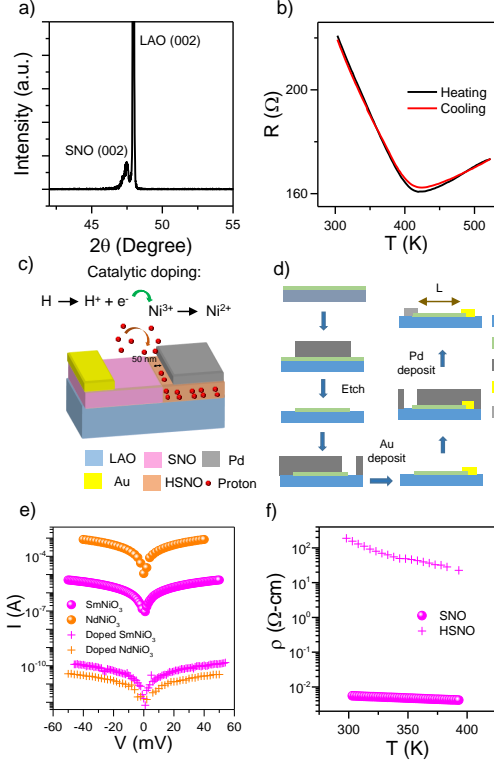


Figure 1. a) XRD of a thin film of SNO (50 nm) grown on LAO substrate. b) Thermal insulator-metal transition in thin film of un-doped SNO/LAO showing the expected transition around 402 K. c) Mott memory device with electrode-selective proton incorporation by catalytic doping at Pd/SNO interface. d) Process flow diagram for fabrication of memory device with asymmetric electrode configuration (PR : Photoresist). For symmetric devices, both electrodes are chosen to be Pd. e) Typical IV curves for pristine (SNO & NNO) and protonated regions (Doped SNO & Doped NNO) showing a large increase in the resistance due to proton incorporation. f) Temperature dependence of resistance of a typical device (encapsulated with 15 nm SiO₂ passivation layer) before and after doping (HSNO) indicating stability of protons in the lattice.

into the device by annealing them under forming gas at 100°C for about 15 minutes in a home built furnace. The dopants are localized close to the catalytic Pd electrode and can re-distribute under electric bias thereby changing the resistance of the channel. The moderate temperature annealing conditions ensures the dopants are incorporated into the lattice in a non-volatile manner.

To understand the electrical behavior before and after doping, IV characteristics of the devices (both SmNiO₃ & NdNiO₃) are shown in Fig. 1e. The presence of Ni²⁺ after proton-electron doping exhibits strong electronic correlations [5] leading to a massive increase in resistance of the material by several orders of magnitude (Fig. 1e). This is due to a large increase in bandgap of the order of 3 eV due to localization upon half-filling (doubly occupied e_g state). The extent of resistance modulation is governed by the voltage-driven diffusion process of protons (that reside in interstitial sites in the perovskite lattice) and so can be varied. This is also the elementary mechanism for designing multiple resistance levels in a memory cell. Fig. 1f shows the dependence of resistance on temperature for both the pristine (SNO) and

proton doped films (HSNO), passivated by 15 nm SiO₂ layer, indicating the stability of protons in these materials. The experiment for resistive switching is performed in a shielded probe station equipped with Keithley 4200 Semiconductor parameter analyzer with a pulse generation unit and a remote amplifier switch that connects between pulse generator and source measuring unit (SMU). The resistance state of the devices is read from the IV response by restricting the voltage levels to within ± 50 mV.

III. RESULTS AND DISCUSSION

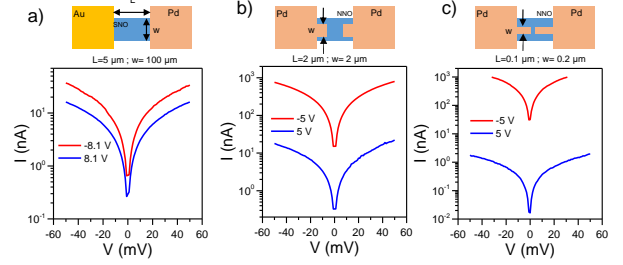


Figure 2. a) IV curve of the device ($L = 5 \mu\text{m}$) after application of pulses (amplitude $= \pm 8.1$ V, duration = 130 ns) along with the device schematic. b) IV curve of another device ($L = 2 \mu\text{m}$) after application of pulses (amplitude $= \pm 5$ V, duration = 30 ns) along with the device schematic. c) IV curve of a sub-micron device ($L = 0.1 \mu\text{m}$) after application of pulses (amplitude $= \pm 5$ V, duration = 100 ns) along with the device schematic.

The IV curves of a typical cell corresponding to HRS (blue curve) and LRS (red curve) is shown in Fig. 2a-c for devices with different channel dimensions along with their schematics. The device, initially in HRS is switched to LRS by application of a pulse of negative amplitude. While the micro scale device ($L = 5 \mu\text{m}$) showed switching from $R_{\text{High}} = 3.3 \text{ M}\Omega$ to $R_{\text{Low}} = 1.5 \text{ M}\Omega$ for a pulse of amplitude -8.1 V and duration of about 130 ns, the sub micron device ($L = 0.1 \mu\text{m}$) showed a larger change in resistance from $R_{\text{High}} = 29.2 \text{ M}\Omega$ to $R_{\text{Low}} = 31.7 \text{ k}\Omega$ for a pulse of amplitude -5 V and duration of about 100 ns. The resistance switching ratio ($R_{\text{High}}/R_{\text{Low}}$) is about 920 for a sub-micron device as compared to 2.2 in a micro scale device. In a device with intermediate length ($L = 2 \mu\text{m}$), the switching ratio is about 43 (Fig. 2b). Note that in micron-scale devices, several volts (over longer duration) are required to provide sufficient driving force, while this scales with the junction dimensions as discussed in the next paragraph. We have also observed resistive switching at 30 ns timescale in our devices as shown in Fig. 2b. Additional experiments to characterize the nature of switching i.e. the effects of applied pulse voltage and duration and test for non-volatility have been performed on representative devices.

We have measured the switching ratio as a function of pulse duration keeping the amplitude constant (± 9.1 V) (Fig. 3a) and as a function of pulse voltage keeping the pulse duration constant (540 ns) (Fig. 3b). We observe a linear scaling of switching ratio as the pulse duration and voltage increase. This seems to suggest that the process of switching is governed by energy supplied to displace the protons. To confirm this, we plot V^2t as a function of switching ratio (Fig. 3d), where we

Table I
COMPARISON OF THE RELEVANT METRICS REPORTED FOR PROTON-DOPED RESISTIVE SWITCHING DEVICES

Material	Doping method	Switching time scale	Channel length	Switching voltage	Switching Ratio	Ref
WO ₃	Diffusion (hygroscopic film)	~ 2 minutes	> 500 μm	10 V	10	[6]
NdNiO ₃	Catalytic doping	~ 5 milli seconds	~ 700 μm	1 V	10	[7]
SiO _x	Proton exchange reaction	~ 10 micro seconds	2 μm	~ 5 V	100	[8]
NdNiO ₃	Catalytic doping	~ 30 nano seconds	0.1 μm	5 V	920	This work

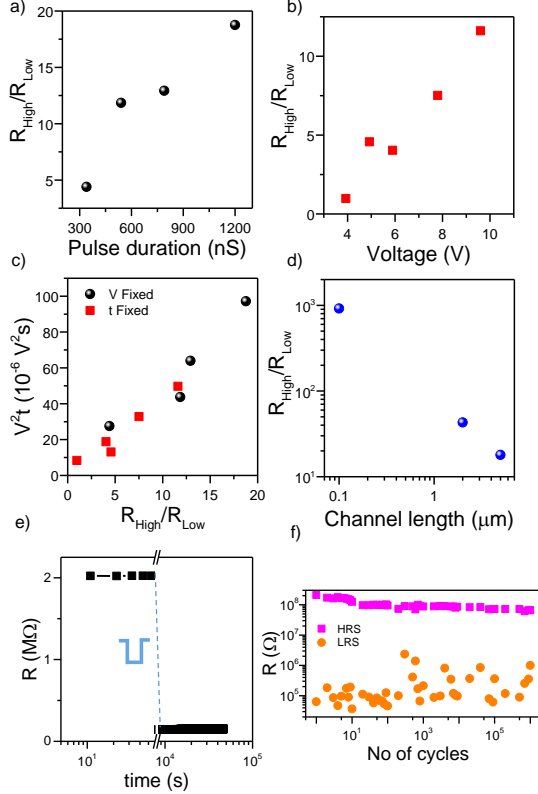


Figure 3. a) Switching ratio as a function of different pulse duration at 9.1 V in a RRAM cell. b) Switching ratio as a function of applied pulse voltages with pulse duration of 540 ns. The switching ratio scales with pulse width and duration due to larger displacement of protons in the channel. c) Scaling of V^2t as a function of switching ratio indicates that larger switching ratio is achieved by supplying larger energy to the devices. d) Scaling in Mott memory: Maximum value of switching ratio for devices as a function of channel length. e) Non-volatility test of memory device. The LRS is retained for more than 11 hours. f) Endurance test of cell (passivated with 15 nm SiO₂) switched using pulses of duration 100 ns and amplitude ± 5 V. The device is stable for $> 10^6$ cycles.

see that the data in plots in Fig. 3a,b collapse on to each other and the linear scaling shows that the switching ratio for the device increases with applied energy. The switching ratio also scales with the device dimensions as shown in Fig. 3d where the maximum value increases as the channel length is reduced. We also note that protons possessing smaller ionic radii than oxygen ions or cations cause less distortions in the underlying lattice. This may translate eventually into lower activation energy for ion-driven switching.

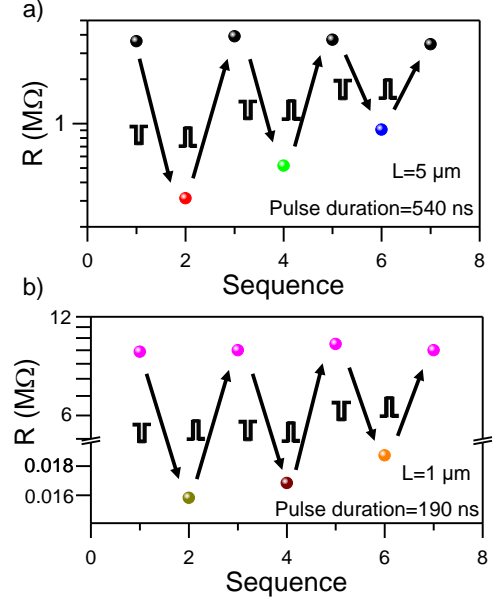


Figure 4. a) Multi-state switching demonstrated in a device with $L = 5\mu\text{m}$. Re-distribution of protons across the device by application of different voltage bias ($V = -5.9$ V, -7.8 V, -9.6 V for LRS and $V = 9.6$ V for HRS, pulse duration = 540 ns) enables multi-states. The resistance ratio for a given switching time can be increased in smaller gap devices by extending the regime of electron doping in the channel. b) As an example multi-state switching is demonstrated in a device with $L = 1\mu\text{m}$ ($V = -8$ V, -9 V, -10 V for LRS and 10 V for HRS, pulse duration = 190 ns).

We then evaluate non-volatile behavior in the cells (Fig. 3e). The device (initially in HRS) is switched to LRS and the resistance is monitored continuously in the LRS. The change in the resistance (in LRS) is less than 15 % measured over 11 hours. In Fig. 3f, we show results of an endurance test performed on a device with a switching time of 100 ns and pulse voltage of ± 5 V and find that the device is stable over 10^6 cycles which is an encouraging initial result. Future studies are necessary to better understand the reliability and endurance properties of such Mott devices. A comparison with literature reports on proton doped oxides [6]–[8] exhibiting resistive switching (Tab. I) indicate that our devices show higher speed and switching ratio, thus suggesting that filling-controlled Mott transition based nickelate memory is an interesting candidate among new materials being considered for emerging memory technologies.

We have further studied multi-level operation by switching

to various resistance states by varying the applied pulse voltage while keeping the pulse duration fixed at 540 ns (Fig. 4a). The device is initially in HRS ($R \sim 2.5 \text{ M}\Omega$) and switched to LRS ($R \sim 300 \text{ k}\Omega$) with -9.6 V pulse. The device is then taken back to its HRS by 9.6 V pulse. Then the device is sequentially taken through various resistance states in sequence by tuning the pulse amplitude. Fig. 4b shows the multi-level switching of another device ($L = 1 \text{ }\mu\text{m}$) with pulse duration of 190 ns.

IV. CONCLUSIONS

We have demonstrated pulsed voltage-driven resistance switching in proton-doped perovskite nickelates. Under voltage bias, the protons rapidly re-distribute leading to distinct resistance states. The results suggest the physical phenomena of orbital filling-controlled Mott transition in correlated oxides can be relevant for emerging memory devices.

REFERENCES

- [1] D. Ielmini and R. Waser, *Resistive Switching: From Fundamentals of Nanoionic Redox Processes to Memristive Device Applications*. John Wiley & Sons, 2015.
- [2] H. Akinaga and H. Shima, "Resistive random access memory (reram) based on metal oxides," *Proceedings of the IEEE*, vol. 98, no. 12, pp. 2237–2251, 2010.
- [3] S. Middey, J. Chakhalian, P. Mahadevan, J. Freeland, A. J. Millis, and D. Sarma, "Physics of ultrathin films and heterostructures of rare-earth nickelates," *Annual Review of Materials Research*, vol. 46, pp. 305–334, 2016.
- [4] S. Catalano, M. Gibert, J. Fowle, J. Íñiguez, J. Triscone, and J. Kreisel, "Rare-earth nickelates RNiO₃: thin films and heterostructures," *Reports on Progress in Physics*, vol. 81, no. 4, p. 046501, 2018.
- [5] J. Shi, Y. Zhou, and S. Ramanathan, "Colossal resistance switching and band gap modulation in a perovskite nickelate by electron doping," *Nature communications*, vol. 5, p. 4860, 2014.
- [6] S. Thakoor, A. Moopen, T. Daud, and A. Thakoor, "Solid-state thin-film memistor for electronic neural networks," *Journal of Applied Physics*, vol. 67, no. 6, pp. 3132–3135, 1990.
- [7] C. Oh, S. Heo, H. M. Jang, and J. Son, "Correlated memory resistor in epitaxial NdNiO₃ heterostructures with asymmetrical proton concentration," *Applied Physics Letters*, vol. 108, no. 12, p. 122106, 2016.
- [8] Y.-F. Chang, B. Fowler, Y.-C. Chen, F. Zhou, C.-H. Pan, T.-C. Chang, and J. C. Lee, "Demonstration of synaptic behaviors and resistive switching characterizations by proton exchange reactions in silicon oxide," *Scientific reports*, vol. 6, p. 21268, 2016.